Infrared and Raman spectra of β-BC_2N from first principles calculations

Jian Sun, Xiang-Feng Zhou, Jing Chen, Ya-Xian Fan, and Hui-Tian Wang*
National Laboratory of Solid State Microstructures and Department of Physics, Nanjing University, Nanjing 210093, China

Xiaoju Guo, Julong He, and Yongjun Tian
Key Laboratory of Metastable Materials Science and Technology, Yanshan University, Qinhuangdao 066004, China
(Received 25 April 2006; revised manuscript received 2 October 2006; published 1 November 2006)

We present the study on the infrared and nonresonant Raman spectra of β-BC_2N within the framework of *ab initio* pseudopotential density functional perturbation theory in a four-atom orthorhombic unit cell. The Raman tensors are calculated from the second-order response of the electronic density matrix with respect to a uniform electric field. Comparison between experiments and calculations for cubic BN is presented to test our method in reproducing all the measured features quantitatively. The LO/TO splitting is well imposed by adding the nonanalytical part deduced from the Born effective charge and macroscopic dielectric constant. Finally, different Raman experiment configurations for β-BC_2N are discussed.

DOI: 10.1103/PhysRevB.74.193101 PACS number(s): 78.30.−j, 71.15.Mb, 81.05.Zx

Much interest has been paid to the boron-carbon-nitrogen (B-C-N) compounds, since the theoretical studies showed that β-C_3N_4 should have a hardness comparable to diamond.[1] With excellent mechanical performances[2] and electronic properties,[3] the B-C-N compounds may lead to many potential applications. Among these compounds, the cubic phases have gained special attention, because they are expected to be stabler than diamond in chemistry and thermology, and harder than cubic BN (*c*-BN). Some cubic BCN materials have been successfully synthesized[4,5] since the report by Badzian.[6] On the other hand, density functional theory (DFT) has been extensively used to study the structural, electronic, mechanical, and linear optical properties of the B-C-N compounds.[7–10] Infrared (IR) and Raman spectroscopies are two standard, sensitive and widely used techniques in materials science to detect the occurrence of new phases or structural changes. Although some IR and Raman studies of the B-C-N compounds have been reported,[11,12] theoretical prediction of IR and Raman spectra is still of great importance and interesting.

Raman peak position can be predicted by the first-order response, because it depends on the frequency ω of the optical phonon at the Brillouin-zone center (Γ point).[13,14] Peak intensity of the nonresonant Stokes Raman spectrum can be calculated under the Placzek approximation as $I \propto |\hat{e}_i \mathbb{A} \hat{e}_s|^2 \omega^{-1}(u+1)$, where $u=[\exp(\hbar\omega/k_BT)-1]^{-1}$.[15] Here $\hat{e}_i(\hat{e}_s)$ is the polarization of the incident (scattered) radiation, T the temperature and $\mathbb{A}$ the Raman susceptibility tensor with the elements A_{ij}. A_{ij} can be computed from various ways, including the second derivative of the electronic density matrix,[15] the finite differences of the dielectric tensor,[16] and the dynamical autocorrelation functions of the polarizability tensor in a molecular dynamics run.[17] Here we follow the first approach based on the well-known $2n+1$ theorem. Most of calculations are performed with PWSCF code[18] within the framework of *ab initio* pseudopotential density functional perturbation theory (DFPT).[13,14] Norm-conserving pseudopotentials with generalized gradient approximation (GGA) in Troullier-Martins type are employed. Nonlinear core correction (NLCC)[19] is used, since GGA pseudopotentials with Perdew-Burke-Ernzerhof (PBE) parametrization are utilized for exchange correlation. It is well known that, there is no direct relationship between GGA and NLCC. Because the gradient-corrected functionals tend to be ill-behaved when $\rho(r)\to 0$ at large or small r, which may lead to the instability in the generation procedure for pseudopotentials or the occurrence of an unpleasant "spike" at $r\to 0$ in pseudopotentials. Such a problem can be avoided with the core correction.[20] In our calculations, all the structures are relaxed before the calculation of the total energy. A 75 Ry plane wave cutoff energy and $8\times8\times8$ Monkhorst-Pack mesh of points in the Brillouin-zone integration are used. The estimated energy error in self-consistency is less than 10^{-8} (a.u.). The relaxations are performed until the total energy changes less than 10^{-4} (a.u.) between two consecutive self-consistent-field (SCF) steps and all the components of forces are smaller than 10^{-3} (a.u.).

To test our method, we investigated the IR and Raman spectra of *c*-BN. We first calculated the optimized cell parameters, macroscopic dielectric constant ε^{∞}, Born effective charge Z^* and optical phonon modes ω (at Γ point) for *c*-BN, as listed in Table I. It can be found that the cell parameters from GGA are larger than those from LDA, and our GGA results are much closer to the measured values[4] than our LDA ones and other theoretical results.[7,21] Because of the cubic symmetry, the three principal values of Z^* and ε^{∞} are identical and can be described by one single scalar. Our calculation values, $Z^*=1.90$ and $\varepsilon^{\infty}=4.56$, are in good agreement with those reported values of $Z^*=1.89$ (Ref. 24) and $=1.93$,[25] and $\varepsilon^{\infty}=4.54$ (Refs. 24 and 25) and 4.50,[26] respectively.

For the Raman modes, as well known, the LO mode is different from the TO mode that the dipole moment originated from the former could induce a macroscopic electric field parallel to the wave vector, which results in the TO/LO splitting.[13,23] The splitting depends mainly on Z^* and ε^{∞}, and can be determined by adding a nonanalytical part into the dynamical matrix.[13] To give the further evidence, we make a comparison between our calculated IR and Raman spectra and the experimental results for *c*-BN, as depicted in Fig. 1.

 ©2006 The American Physical Society

TABLE I. Optimized cell parameters, macroscopic dielectric constant ε^{∞}, Born effective charge tensor Z^{*} and optical phonon modes ω for c-BN, compared with the calculated and experimental values in the literature.

	a (Å)	ε^{∞}	Z^{*}	ω (cm^{-1})
GGA	3.612	4.56	1.90	(1033, 1270)
	3.596[a]	4.54[d]	1.89[d]	(1062,1295)[d]
LDA	3.548	4.51	1.86	(1099, 1326)
	3.572[b]		1.93[e]	(1040,1285)[e]
Expt.	3.617[c]	4.50[f]		(1056, 1304)
				(1055,1304)[g]
				(1056,1303)[h]

[a]Reference 21.
[b]Reference 7.
[c]Reference 4.
[d]Reference 24.
[e]Reference 25.
[f]Reference 26.
[g]Reference 22.
[h]Reference 27.

Our IR transmittance (Expt-1) measured from a commercial c-BN sample (fineness number 80–100) dispersed in KBr slice, an absorption valley at $\sim$1058 cm^{-1} is observed, the sharp spikes above 1400 cm^{-1} may come from the water vapor or the other noises. Another result (Expt-2) measured from the c-BN thin film in Ref. 11 has a strong absorption valley at $\sim$1065 cm^{-1}. Our Raman measurement excited by the 488 nm Ar^{+} laser line shows the TO and LO modes to be at 1056 and 1304 cm^{-1} (Expt-1), respectively, which are in well agreement with 1055 and 1304 cm^{-1} (Expt-2) of the Raman experiment excited by the 244 nm laser line.[22] Our calculated modes are at 1033 and 1270 cm^{-1} with GGA, and at 1099 and 1326 cm^{-1} with LDA. Such differences originate mainly from the different lattice constants and bond lengths optimized by the two kinds of pseudopotentials. The Raman intensities calculated from GGA are stronger than those from LDA, but the relative magnitudes are almost unchange that agrees with both experimental measurements.

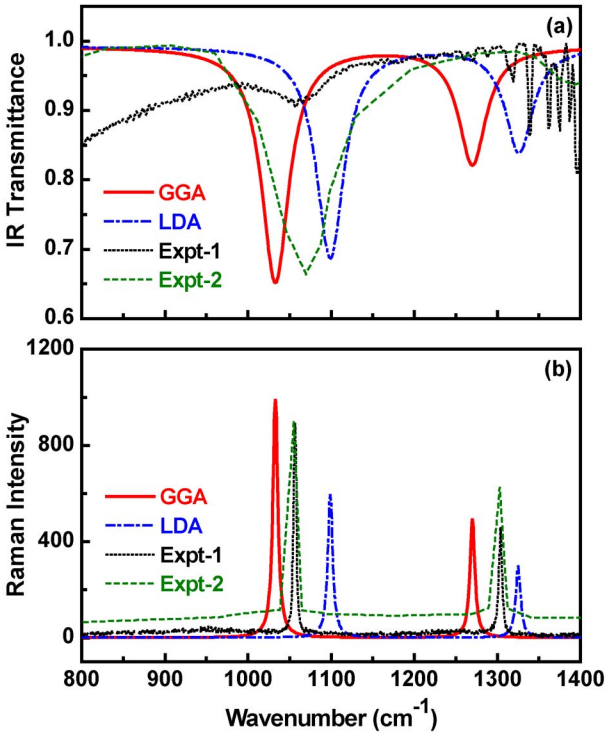

FIG. 1. (Color online) Calculated IR and Raman spectra of c-BN, experimental results are also plotted for comparison (Expt-1 is by ourselves and Expt-2 is from Refs. 11 and 22).

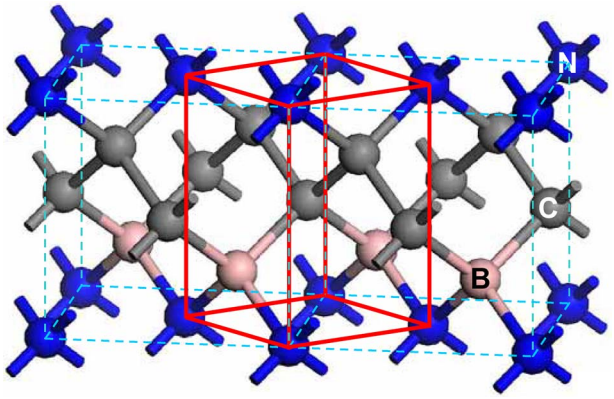

FIG. 2. (Color online) Structure of β-BC_2N, the redefined orthorhombic unit cell is shown by the thick lines while thin dash lines represent the conventional cell.

We now devote to the first-principles calculations of the IR and Raman spectra for β-BC_2N, which is expected to be the most stable one among the seven topologically different phases for cubic BC_2N.[7,8,21] We know that the cubic BC_2N structures including the β phase were predicted from the zinc-blende c-BN with eight-atoms cell, by replacing two B atoms and two N atoms by C atoms. It become monoclinic after relaxation. Therefore β-BC_2N is in general defined as a monoclinic cell composed of eight atoms (as shown by the thin dashed lines in Fig. 2) in the previous works.[7,8,21] In this monoclinic cell, the bond angle β have only a very small deviation from right angle. (β=90.63° from our GGA, β =90.54° from our LDA and β=89.32° in Ref. 21.) We find that it is more proper to define the lattice with a four-atoms orthorhombic unit cell (as shown by the thick solid lines in Fig. 2) when the symmetry restriction ($Pmm2$) is imposed in the process of optimizing the structure. This four-atoms orthorhombic cell is the simplest cell with the least atoms, which is more convenient in calculations. Moreover, we also check that the total energy per formula for these two kinds of lattices are very close (−49.5168 Ry/formula for the four atoms cell and −49.5144 Ry/formula for the eight-atoms cell).

For β-BC_2N, the optimized cell parameters for the eight-atoms and four-atoms cells calculated with GGA and LDA are listed in Table II, together with some other theoretical and experimental results. Our results are close to the previous theoretical prediction.[21] The lattice constants from GGA are larger than that from LDA. Because it is difficult to obtain a pure sample, the experimental values in Refs. 4 and 5 from cubic BC_2N or $C_{0.5}(BN)_{0.5}$ are not exact for β-BC_2N phase. However, those measured values are still close to our results.

TABLE II. Optimized cell parameters for β-BC_2N, compared with the calculated and experimental results in the literature (values measured in Refs. 4 and 5 are for cubic BC_2N, but not pure β-BC_2N).

	GGA	LDA
Mono	$a=c=3.595$, $b=3.631$ ($\alpha=\gamma=90^\circ, \beta=90.63^\circ$)	$a=c=3.532$, $b=3.570$ ($\alpha=\gamma=90^\circ, \beta=90.54^\circ$)
Orth	$a=2.556$, $b=2.528$, $c=3.631$ ($\alpha=\beta=\gamma=90^\circ$)	$a=2.510$, $b=2.486$, $c=3.570$ ($\alpha=\beta=\gamma=90^\circ$)
Calc.[a]	$a=b=3.579$, $c=3.612$ ($\alpha=\beta=90^\circ, \gamma=89.32^\circ$)	
Calc.[b]		$a=3.577$ ($\alpha=89.38^\circ, \beta=\gamma=90.62^\circ$)
Expt.[c]	$a=3.602$	
Expt.[d]	$a=3.642$	

[a]Reference 21.
[b]Reference 7.
[c]Reference 4.
[d]Reference 5.

As shown in Table III, for the four-atoms unit cell, the macroscopic dielectric constant $\varepsilon^{\infty}_{\text{orth}}$ and the Born effective charge Z^{*}_{orth} are indeed diagonal tensors. The principal elements of $\varepsilon^{\infty}_{\text{orth}}$ are [5.98, 5.37, 5.76], and those of Z^{*}_{orth} for the four nonequivalent atoms (B, C, C, and N) are [1.12, 1.37, 1.53], [−1.30, −0.94, −1.14], [1.79, 0.98, 1.16], and [−1.53, −1.41, −1.55], respectively. For the eight-atoms cell, however, $\varepsilon^{\infty}_{\text{mono}}$ and Z^{*}_{mono} are symmetric tensors with nonzero nondiagonal elements, due to the monoclinic lattice. After performing the diagonalization for $\varepsilon^{\infty}_{\text{mono}}$ and Z^{*}_{mono}, we find that the diagonalized tensors are almost the same as $\varepsilon^{\infty}_{\text{orth}}$ and Z^{*}_{orth}, respectively. This is also an evidence that the simplification from the eight-atoms cell to the four-atoms cell is reasonable.

TABLE III. Calculated macroscopic dielectric constant, Born effective charge and optical phonon modes for β-BC_2N with GGA. The irreducible representations are also listed. I and R denotes the IR- and Raman-active modes (cm^{-1}), respectively.

$\varepsilon^{\infty}_{\text{orth}}$	$\begin{bmatrix} 5.98 & 0.00 & 0.00 \\ 0.00 & 5.37 & 0.00 \\ 0.00 & 0.00 & 5.76 \end{bmatrix}$
$\varepsilon^{\infty}_{\text{mono}}$	$\begin{bmatrix} 5.68 & 0.00 & -0.30 \\ 0.00 & 5.75 & 0.00 \\ -0.30 & 0.00 & 5.68 \end{bmatrix}$
Z^{*}_{orth}	$\begin{bmatrix} 1.12 & 0.00 & 0.00 \\ 0.00 & 1.37 & 0.00 \\ 0.00 & 0.00 & 1.53 \end{bmatrix}_{\text{B}} \begin{bmatrix} -1.30 & 0.00 & 0.00 \\ 0.00 & -0.94 & 0.00 \\ 0.00 & 0.00 & -1.14 \end{bmatrix}_{\text{C}}$
	$\begin{bmatrix} 1.79 & 0.00 & 0.00 \\ 0.00 & 0.98 & 0.00 \\ 0.00 & 0.00 & 1.16 \end{bmatrix}_{\text{C}} \begin{bmatrix} -1.53 & 0.00 & 0.00 \\ 0.00 & -1.41 & 0.00 \\ 0.00 & 0.00 & -1.55 \end{bmatrix}_{\text{N}}$
Z^{*}_{mono}	$\begin{bmatrix} 1.23 & 0.00 & 0.12 \\ 0.00 & 1.53 & 0.00 \\ 0.12 & 0.00 & 1.23 \end{bmatrix}_{\text{B}} \begin{bmatrix} -1.15 & 0.00 & 0.19 \\ 0.00 & -1.14 & 0.00 \\ 0.19 & 0.00 & -1.15 \end{bmatrix}_{\text{C}}$
	$\begin{bmatrix} 1.39 & 0.00 & -0.39 \\ 0.00 & 1.16 & 0.00 \\ -0.39 & 0.00 & 1.39 \end{bmatrix}_{\text{C}} \begin{bmatrix} -1.47 & 0.00 & 0.08 \\ 0.00 & -1.55 & 0.00 \\ 0.08 & 0.00 & -1.47 \end{bmatrix}_{\text{N}}$
ω_{orth}	660(B_1,R/I), 705(B_2,R/I), 740(B_1,R/I), 945(B_2,R/I), 1055(A_1,R/I), 1147(A_1,R/I), 1203(B_1,R/I), 1219(B_2,R/I), 1245(A_1,R/I)

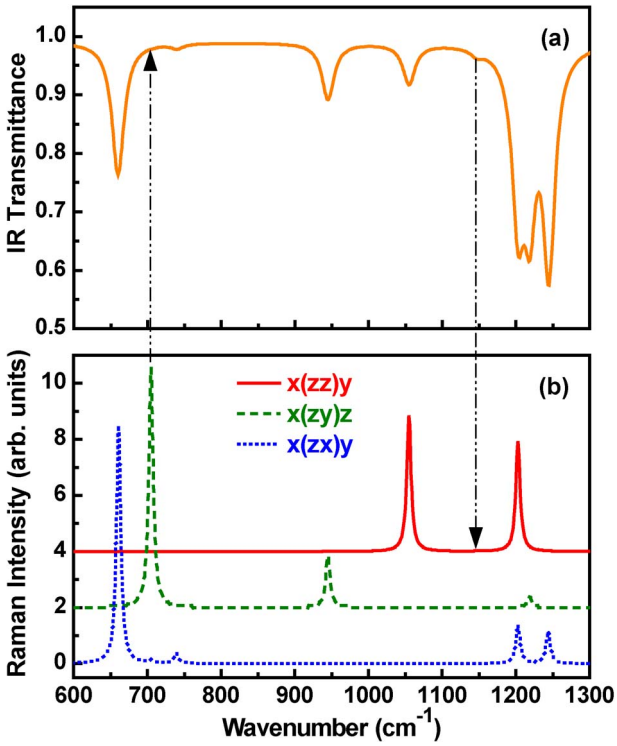

FIG. 3. (Color online) Calculated IR transmittance spectrum (a) and Raman spectra in three different configurations for β-BC_2N.

Inasmuch as the orthorhombic unit cell of β-BC_2N containing four atoms, there should be 12 phonon modes at Γ point, including three acoustic modes and nine optical modes. By the symmetry analysis for the structure of orthorhombic β-BC_2N ($Pmm2$, C_{2v}, $Z=1$) and with the aid of the table of irreducible representations,[28] the nine optical modes at Γ point ($3A_1+3B_1+3B_2$) are simultaneously IR and Raman active, as listed in Table III. The six TO modes are at 660, 705, 740, 945, 1203, and 1219 cm^{-1}. The three LO modes are at 1055, 1147, and 1245 cm^{-1}, they are located at 1028, 1141, and 1181 cm^{-1} before imposing the LO/TO splitting, respectively.

To give an intuitive picture, we calculated the IR transmittance for the orthorhombic unit cell of β-BC_2N, as shown in Fig. 3(a). It can be found that there are four strong absorption modes (at 660, 1203, 1219, and 1245 cm^{-1}), two relatively weak absorption modes (at 945 and 1055 cm^{-1}), two very weak absorption modes (at 740 and 1147 cm^{-1}) and the absorption mode at 705 cm^{-1} is too weak to be observed. To observe all nine Raman modes experimentally, we also pre-

sented the Raman spectra for three typically experimental configurations below, respectively, as plotted in Fig. 3(b).

(i) The $x(zx)y$ configuration. For the incident radiation, its wave vector is along the x axis ($\hat{k}_i=[1,0,0]$) and its polarization is in the z direction ($\hat{e}_i=[0,0,1]$). For the scattered radiation, its wave vector is in the y direction ($\hat{k}_s=[0,1,0]$) and its polarization is parallel to the x axis ($\hat{e}_s=[1,0,0]$). Due to the requirement of the moment conservation, the phonon vector should be in the direction of $\hat{e}_q=[1/\sqrt{2},-1/\sqrt{2},0]$. The five Raman modes could be detected at 660, 705, 740, 1203, and 1245 cm^{-1}. However, the Raman modes at 705 and 740 cm^{-1} are too weak.

(ii) The $x(zy)z$ configuration. We have $\hat{k}_i=[1,0,0]$, $\hat{e}_i=[0,0,1]$, $\hat{k}_s=[0,0,1]$, and $\hat{e}_s=[0,1,0]$. The phonon provides the exchanged momentum, which means $\hat{e}_q=[1/\sqrt{2},0,-1/\sqrt{2}]$. We find three Raman modes at 705, 945, and 1219 cm^{-1}, respectively; the mode at 1219 cm^{-1} is very weak.

(iii) The $x(zz)y$ configuration. In this case, there are $\hat{k}_i=[1,0,0]$, $\hat{k}_s=[0,1,0]$, and $\hat{e}_i=\hat{e}_s=[0,0,1]$. The momentum of phonon should be $\hat{e}_q=[1/\sqrt{2},-1/\sqrt{2},0]$. There should be three Raman modes, in which two Raman peaks at 1055 and 1203 cm^{-1} are strong, the residual at 1147 cm^{-1} is too weak to be distinguished.

In summary, we study the IR and Raman spectra of β-BC_2N with a four-atoms orthorhombic unit cell. Symmetry analysis shows that all the optical phonon modes at the Brillouin zone center are both IR and Raman active. Macroscopic dielectric tensors and Born effective charge tensors for the four-atoms orthorhombic and eight-atoms monoclinic cells are studied and found to be very similar, showing that our simplification is viable. The present results are based on the ordered structure of β-BC_2N. In experiment, however, most ternary B-C-N samples prepared by the high-pressure and high-temperature method are powder or tiny crystals composed by many different kinds of phases. For the fact that the single crystalline β-BC_2N is difficult to synthesize, one should be very careful to compare our results directly with experimental values.

The authors gratefully appreciate the generous help from M. Lazzeri and P. Giannozzi in calculations, and G. S. Huang, J. X. Zhou, and P. Zhan in experiments. This work was partially supported by the National Natural Science Foundation of China (Grants Nos. 10325417, 90501006 and 50532020).

*Electronic address: htwang@nju.edu.cn

[1] A. Y. Liu and M. L. Cohen, Science **245**, 841 (1989); A. Y. Liu and M. L. Cohen, Phys. Rev. B **41**, 10727 (1990).
[2] F. M. Gao, J. L. He, E. R. Wu, S. M. Liu, D. L. Yu, D. C. Li, S. Y. Zhang, and Y. J. Tian, Phys. Rev. Lett. **91**, 015502 (2003).
[3] J. L. He, Y. J. Tian, D. L. Yu, T. S. Wang, S. M. Liu, L. C. Guo, D. C. Li, X. P. Jia, L. X. Chen, G. T. Zou, and O. Yanagisawa, Chem. Phys. Lett. **340**, 431 (2001).
[4] E. Knittle, R. B. Kaner, R. Jeanloz, and M. L. Cohen, Phys. Rev. B **51**, 12149 (1995).
[5] V. L. Solozhenko, D. Andrault, G. Fiquet, M. Mezouar, and D. C. Rubie, Appl. Phys. Lett. **78**, 1385 (2001).
[6] A. R. Badzian, Mater. Res. Bull. **16**, 1385 (1981).
[7] Y. Tateyama, T. Ogitsu, K. Kusakabe, S. Tsuneyuki, and S. Itoh, Phys. Rev. B **55**, 010161 (1997).
[8] H. Sun, S. H. Jhi, D. Roundy, M. L. Cohen, and S. G. Louie, Phys. Rev. B **64**, 094108 (2001); J. Sun, X. F. Zhou, Y. X. Fan, J. Chen, H. T. Wang, X. J. Guo, J. L. He, and Y. J. Tian, *ibid.* **73**, 045108 (2006).
[9] Y. N. Xu and W. Y. Ching, Phys. Rev. B **44**, 7787 (1991).
[10] J. Sun, H. T. Wang, N. B. Ming, J. L. He, and Y. J. Tian, Appl. Phys. Lett. **84**, 4544 (2004).
[11] S. Kidner, C. A. Taylor II, and R. Clarke, Appl. Phys. Lett. **64**, 1859 (1994).
[12] S. Itoh, Diamond Films Technol. **7**, 195 (1997); H. W. Hubble, I. Kudryashov, V. L. Solozhenko, P. V. Zinin, S. K. Sharma, and L. C. Ming, J. Raman Spectrosc. **35**, 822 (2004).
[13] S. Baroni, S. de Gironcoli, A. D. Corso, and P. Giannozzi, Rev. Mod. Phys. **73**, 515 (2001).
[14] X. Gonze and C. Lee, Phys. Rev. B **55**, 10355 (1997).
[15] M. Lazzeri and F. Mauri, Phys. Rev. Lett. **90**, 036401 (2003).
[16] S. Baroni and R. Resta, Phys. Rev. B **33**, 5969 (1986); P. Umari, X. Gonze, and A. Pasquarello, Phys. Rev. Lett. **90**, 027401 (2003).
[17] A. Putrino and M. Parrinello, Phys. Rev. Lett. **88**, 176401 (2002).
[18] www.pwscf.org
[19] S. G. Louie, S. Froyen, and M. L. Cohen, Phys. Rev. B **26**, 1738 (1982).
[20] P. Giannozzi (private communication).
[21] R. Q. Zhang, K. S. Chan, H. F. Cheung, and S. T. Lee, Appl. Phys. Lett. **75**, 2259 (1999).
[22] S. Reich, A. C. Ferrari, R. Arenal, A. Loiseau, I. Bello and J. Robertson, Phys. Rev. B **71**, 205201 (2005).
[23] M. Born and K. Huang, *Dynamical Theory of Crystal Lattice* (Oxford University Press, Oxford, 1988), pp. 82–89; J. Lazewski, K. Parlinski, W. Szuszkiewicz, and B. Hennion, Phys. Rev. B **67**, 094305 (2003).
[24] N. Ohba, K. Miwa, N. Nagasako, and A. Fukumoto, Phys. Rev. B **63**, 115207 (2001).
[25] K. Karch and F. Bechstedt, Phys. Rev. B **56**, 7404 (1997).
[26] P. J. Gielisse, S. S. Mitra, J. N. Plendl, R. D. Griffis, L. C. Mansur, R. Marshall, and E. A. Pascoe, Phys. Rev. **155**, 1039 (1967).
[27] O. Brafman, G. Lengyel, and S. S. Mitra, Solid State Commun. **6**, 523 (1968).
[28] G. Y. Zhang, G. X. Lan, and Y. F. Wang, *Lattice Vibration Spectroscopy*, 2nd ed. (High Education Press, Beijing, 2001), pp. 353 (in Chinese).